Applied Catalysis B: Environmental 334 (2023) 122817

Contents lists available at ScienceDirect

Applied Catalysis B: Environmental

journal homepage: www.elsevier.com/locate/apcatb

Temporal analysis of products (TAP) reactor study of the dynamics of CO_2 interaction with a Ru/γ-Al_2O_3 supported catalyst

Corinna Fauth [a], Anja Lenzer [a], Ali M. Abdel-Mageed [a,b], R. Jürgen Behm [a,c,*]

[a] Institute of Surface Chemistry and Catalysis, Ulm University, D-89069 Ulm, Germany
[b] Leibniz Institute for Catalysis (LIKAT Rostock), D-18059 Rostock, Germany
[c] Institute of Theoretical Chemistry, Ulm University, D-89069 Ulm, Germany

ARTICLE INFO

Keywords:
CO_2 reduction
Active oxygen deposition
Oxygen exchange
Ru/Al_2O_3 catalyst
Temporal analysis of products (TAP)

ABSTRACT

As part of a comprehensive study on the reduction of CO_x on supported Ru catalysts we systematically investigated the dynamic interaction of CO_2 with a Ru/γ-Al_2O_3 catalyst in a temporal analysis of products (TAP) reactor, focusing on the redox properties of the catalyst, specifically on the deposition of active oxygen (O_{act}) from CO_2. This was investigated by exposing the pre-reduced catalyst to CO_2 pulses and subsequent titration of the deposited O_{act} by CO pulses. CO_2 is much less active for O_{act} deposition than O_2. Reductive co-reactants reduce (CO) or increase (H_2) the activity of CO_2 for O_{act} deposition. ^{18}O-marked CO_2 pulses show facile oxygen exchange of CO_2 with the catalyst, despite the inertness of the support. Based on excess effluent CO_2 we conclude that surface carbonates can both build up on the surface upon interaction with CO or CO_2 and also decompose upon O_2 or CO_2 pulsing, releasing additional CO_2.

1. Introduction

The interaction of CO_2 with supported Ru catalysts is a crucial and possibly decisive step in a variety of highly important catalytic reactions, such as the methanation of CO_2 [1–7], e.g. for power-to-gas (P2G) applications [8], the selective methanation of CO in CO_2-rich feed gases for fuel cells (feed gas purification) [1,9–11], the Fischer-Tropsch reaction [12–18], or the reverse water-gas shift reaction (RWGS)[19–21]. In these reactions CO_2 can act as reactant in an associative pathway, e.g., via the formation of adsorbed formates during CO_2 hydrogenation [22,23], or alternatively dissociate, leaving O_{ad} on the surface [24]. The latter case would be the first step for a reaction proceeding via a redox mechanism on the Ru nanoparticles (NPs). Ru differs from other transition metals by its very strong bond and affinity to oxygen [25,26], while adsorption energies to small molecules such as CO or CO_2 are comparable to / or only slightly stronger than those observed for noble metals such as Pt [27–30]. As shown previously, the reactivity of the Ru NPs for CO_x methanation is furthermore modified by structural and electronic effects such as the coordination of the Ru atoms contributing to the adsorption site (structural effects) or electronic modifications due to charge transfer from the support to the Ru NP (electronic metal-support interactions – EMSIs) [31–33], more specifically to Ru atoms directly at the metal-oxide interface [33]. Electronic modifications of supported metals are particularly important for Ru catalysts consisting of Ru NPs supported on reducible oxides such as CeO_2, ZrO_2, and TiO_2. These catalysts show a high activity for this reaction compared to those supported on non-reducible oxides such as Al_2O_3 [34], which was attributed to the formation of oxygen vacancies at the metal-support interface, and pronounced electronic metal support interactions (EMSIs) [35,36]. Interestingly, the CO_x methanation activity of Ru/γ-Al_2O_3 was significantly enhanced by a high-temperature treatment in reaction gas ($CO/CO_2/H_2$ or CO_2/H_2). This was explained by a special type of metal-support interactions (MSI), involving a stronger interaction of Lewis basic sites on γ-Al_2O_3, which leads to a flattening of the Ru NPs, in conjunction with an increasing reduction to metallic Ru atoms [37].

In spite of considerable efforts, however, a detailed picture of the interaction of CO_2 with Ru or with supported Ru catalysts does not exist yet. In particular, there is a lack of insights into the Ru redox properties in the interaction with CO_2 (deposition of active oxygen) and its role not only in the formation, but also in the decomposition of surface species upon interaction with CO_2. Among others, this is limited by the too low sensitivity of most analytic methods for the detection of small changes in the surface redox state (< 10%). This is topic and objective of the present

* Corresponding author at: Institute of Theoretical Chemistry, Ulm University, D-89069 Ulm, Germany.
E-mail address: juergen.behm@uni.-ulm.de (R. Jürgen Behm).

https://doi.org/10.1016/j.apcatb.2023.122817
Received 6 March 2023; Received in revised form 20 April 2023; Accepted 25 April 2023
Available online 26 April 2023

paper, where we employed for the temporal analysis of products (TAP) experiments to investigate the dynamic interaction of CO_2 with a supported Ru catalyst, in this case a Ru/γ-Al_2O_3 catalyst. This allows us to quantitatively monitor changes in the catalyst surface related to the deposition and desorption of even small amounts of species such as reaction products or side products on/from the catalyst surface on a very sensitive scale.

In the first step we determined the removal and re-deposition of active oxygen (O_{act}) from the pre-oxidized catalyst by sequences of CO and O_2 pulses, to determine its capacity for O_{act} uptake/release. Temperature effects were explored by performing these experiments at three different temperatures (190 °C, 250 °C, and 300 °C), which are in the range of low- to moderate-temperature CO_2 hydrogenation reactions under typical conditions. Next, we explored the deposition of active oxygen during CO_2 pulses and its subsequent removal by following CO pulse sequences. From the mass balance of the resulting CO_2 and CO we also gain access to the formation and decomposition of surface species formed by reaction of CO_2 with the catalyst surface. The effect of reducible co-reactants such as CO or H_2, which is relevant, e.g., for the Selective Methanation of CO, for the RWGS reaction, or for the CO_2 methanation, is investigated as well. Finally, detailed information on the dynamic oxygen exchange is obtained by using isotope labelling experiments. Exposing the pre-reduced (by CO pulsing), non-labelled catalyst to $C^{18}O_2$ pulses we monitored the isotope composition of the effluent CO_2 pulses. The dynamic evolution of the isotope composition does not only give insight into the facileness of oxygen exchange under these conditions, at 190 °C, but also provides information on the nature of the exchanging surface species and on the distribution of the exchanged oxygen on the surface. Overall, these experiments provide detailed insights into the dynamics of the interaction of CO_2 with Ru/Al_2O_3 catalysts under conditions typical and thus relevant for CO_2 hydrogenation reactions.

2. Experimental

2.1. Temporal analysis of products (TAP) reactor

In all measurements we used a commercial 5 wt% Ru/γ-Al_2O_3 catalyst supplied by Johnson Matthey, UK, (100 $m^2\,g_{cat}^{-1}$, 48% dispersion, 2–3 nm average Ru particle diameter, for further details see [38–40]). Prior to the TAP measurements the catalyst was additionally pretreated in a 10% O_2/N_2 atmosphere at 150 °C for 30 min (O150), in order to remove carbon-containing species on the surface such as formates or carbonates and thus ensure a well-defined starting state and the comparability to previous results [41,42]. Based on previous experiments on a 2.3 wt% Ru/γ-Al_2O_3 [37] the catalyst was fully oxidized after this treatment. The gases used in the pulse experiments were obtained from MTI IndustrieGase (Ar 4.6, CO 4.7, O_2 5.0, CO_2 5.0), Germany, Messer (H_2 6.0), Germany, and Campro Scientific ($C^{18}O_2$ 99%, 95 atom % ^{18}O), Germany.

The multi-pulse and temperature programmed desorption (TPD) experiments were performed in a home-built TAP reactor, which is described in detail in reference [43] and which is based on the TAP-2 approach by Gleaves et al. [44]. The main advancement was the use of two independently working, piezoelectrically driven pulse valves. These generate pulses of approx. $3.2\bullet10^{16}$ molecules per pulse (CO/Ar pulses) and 1.5×10^{16} molecules per pulse (O_2/Ar, CO_2/Ar, CO/CO_2/Ar, H_2/CO_2/Ar, and $C^{18}O_2$/Ar pulses) (pulse length = 50 ms) with high reproducibility during a pulse sequence. The pulses were directed into a tubular quartz glass reactor (215 mm long, 4.0 mm i.d., 6.0 mm o.d.), which contains the three-zone catalyst bed fixed by two stainless steel sieves (Haver & Boecker OHG; aperture 25 μm, transmission 25%). The active zone containing 25 mg of the diluted Ru/γ-Al_2O_3 catalyst (1:4 diluted by α-Al_2O_3) is surrounded by two inert zones comprising 25 mg (incoming side) and 100 mg (effluent side) of SiO_2, respectively. This results in a catalyst bed length of approx. 15 mm in total. Gaseous species, which had passed the micro-reactor or had been formed therein, were analyzed by a quadrupole mass spectrometer (QMG 700, Pfeiffer Vacuum). The mass spectrometer is located in the analysis chamber, which is connected to the end of the micro-reactor via a home-built differentially pumped gate valve [43]. The background pressure in the analysis chamber was approx. 8×10^{-9} mbar, which increased to about 1×10^{-7} mbar during pulsing. In the micro-reactor the background pressure was also about $8\bullet10^{-9}$ mbar. Ar was included in the gas mixture as a calibration standard, allowing to quantitatively evaluate the consumption of CO molecules (or O_2, respectively) of each pulse (see below).

The number of molecules per pulse was determined for each pulse valve by following the pressure drop in the respective gas tank during a sequence of rapidly following Ar pulses at different Ar pre-pressures. For CO, O_2 and CO_2 this was calculated via the molar mass of these gases, assuming that the pulse size is determined by the respective impingement rate. From technical reasons, the first two pulses in a sequence are considerably smaller than the subsequent ones. The specific cross sections of the different gases in the mass spectrometric measurements were calculated from the signals obtained for a certain partial pressure of the respective gases, which were directly injected into the analysis chamber at different pre-pressures.

2.2. Multi-pulse experiments

Multi-pulse reduction / oxidation experiments after O150 pretreatment were performed by sending CO/Ar (molecular ratio 1:1) pulses over the catalyst bed to remove active oxygen (O_{act}) species. The number of pulses was chosen such that in the end of the sequence there was no significant change in the detected signals anymore. The separation time (Δt) between pulses was adjusted such that the next pulse started after the Ar signal of the preceding pulse had completely decayed to the background signal. This is followed by a similar type oxidation experiment, where we admitted a sequence of O_2/Ar (1:1) pulses to the catalyst.

The resulting pulse size was determined by integration of the mass spectroscopic signal during the time of the pulse, after the subtraction of the background signal. For the integrated signal intensity of CO (m/z = 28) or CO_2 (m/z = 44), the fragmentation of CO_2^+, which results in the formation of CO^+ and therefore contributes to the CO signal intensity, was considered in the evaluation. In a blank measurement of CO_2/Ar pulsing over inert α-Al_2O_3 the fragmentation of CO_2 was determined to be 13%. This contribution from CO_2 fragmentation was added to the resulting CO_2 signal intensity and deducted from the CO signal intensity. In the case of reactants and products this includes small contributions from the preceding pulse. These are largely compensated, however, by similar size contributions of the present pulse to the measured signal of the subsequent pulse. To remove effects of fluctuations in the incoming pulse sizes, the consumption of reactive gas per pulse was determined by subtracting the measured intensity of the outgoing pulse from an intensity of the incoming pulse that was calculated from the Ar signal of this pulse and the average CO : Ar intensity ratio measured after saturation. To obtain the total amount of oxygen storage and removal, the amount of CO or O_2 consumed in each pulse of the sequence was accumulated. These reduction / oxidation multi-pulse experiments were performed at 190 °C, 250 °C, and 300 °C, respectively.

Due to technical limitations in the size of the resulting data files we had to split the complete multi-pulse sequence into separate subsequences of 180 pulses each. The first pulse of the sub-sequence n + 1 was sent approx. 5 min after the last pulse of the preceding subsequence n. This break time was used also to determine the background signal at the end and at the beginning of a measurement, respectively. The start of a new sub-sequence often led to a change of the respective pulse signal, in addition to the much smaller size of the first two gas pulses in each sub-sequence (see above). Both effects are particularly obvious for the CO_2 signal. Therefore, we re-calibrated the

CO_2 pulse size in the later sub-sequences such that they exhibited a continuous trend.

Multi-pulse experiments including CO_2 in the pulsed atmosphere, which were performed to evaluate the relative oxidation power of CO_2 as compared to O_2, were conducted with CO_2/Ar (1:2) pulses and with gas mixtures containing also a reducing agent (CO/CO_2/Ar (1:1:1) and H_2/CO_2/Ar (1:1:1)). In all cases pulses of the gas mixture were admitted at 190 °C to the pre-reduced catalyst, after O150 treatment and CO pulsing.

Experiments using isotope labelled gases were performed using $C^{18}O_2$ (Campro Scientific, purity 99%, 95 atom% ^{18}O). In contrast to unlabeled CO_2 this allows to also detect reversible interaction between CO_2 and the catalyst surface, if this results in the exchange of single oxygen atoms.

2.3. TAP-based temperature programmed desorption (TAP-TPD)

TPD measurements were performed in the TAP set-up directly after the multi-pulse experiments. The catalyst was heated from the reaction temperature of 190 °C to 450 °C (25 °C min^{-1}). After keeping the temperature for 5 min, the catalyst was cooled to the initial temperature again (25 °C min^{-1}). The desorbing gases entered the analysis chamber, where they were detected by the mass spectrometer. Here, we used the same conversion of the mass spectrometric signals of CO, CO_2 and O_2 into numbers of molecules as described above. For the H_2O signal we used the ratio of the tabulated sensitivity factors for Ar and H_2O and the experimentally determined sensitivity factor of Ar (see above).

2.4. Quasi in-situ X-ray photoelectron spectroscopy (XPS)

Quasi in-situ XPS measurements were performed after an O150 pretreatment and additional 1000 pulses of CO/Ar or CO_2/Ar, in order to analyze the build-up of surface adsorbates such as surface carbonates during pulsing. To minimize contamination effects the catalyst transfer from the micro-reactor into the XPS chamber was carried out without exposing the catalyst to air.

The measurements were carried out using a PHI 5800 ESCA system (Physical Electronics) with monochromatized Al-K_α radiation (1486 eV) equipped with a neutralizer (flood gun) for charge compensation. The binding energies (BEs) of all spectra were calibrated against that of the C 1s peak of residual carbon (284.8 eV) [45]. Survey spectra were recorded using a pass energy of 93.9 eV, detail spectra with 29.35 eV. Deconvolution of the signals was performed using the software CASAXPS Version 2.3.23 Pr1.0 (Casa Software Ltd.). The peak widths of the C 1s components were limited to 1.5 and 2.0 eV. The deconvolution of the Ru 3d (spin-orbit splitting of 4.17 eV) and C 1s components was carried out by using three different Ru species (Ru^0, Ru^{4+}, and Ru^{3+}). The BEs of the Ru^0 and Ru^{4+} species were fixed at 280.1 ± 0.1 eV and 280.9 eV (shifted by 0.8 eV to higher BE), respectively. A third state at 282.1 ± 0.1 eV is assigned to a satellite state of the Ru^{4+} state in RuO_2 or to Ru^{3+} species, e.g., in hydroxylated $RuO_2/Ru(OH)_3$. Details for the Ru 3d binding energies and XPS data can be found in ref. [46].

The catalyst sample was mounted on a carbon containing glue pad. To avoid contamination by contact with air after pretreatment or after the multi-pulse measurements, the catalyst sample transfer was performed via a transfer cell. After the catalyst pretreatment (O150) or after additional 1000 pulses CO/Ar, the microreactor was vented by Ar, disconnected from the TAP reactor, sealed off with Parafilm and filled with N_2. The reactor was then transferred to a glove box, there the catalyst sample was removed and loaded into a special XPS transfer cell, which was filled with Ar. Subsequently, the transfer cell was transported to the XPS system and connected to the load lock. This way, the sample was never exposed to the ambient atmosphere during transfer, and changes in the surface composition induced by exposure to the atmosphere could be excluded. This procedure was used for both measurements shown in Fig. S5 (C 1s, Ru 3d).

3. Results

3.1. Active oxygen removal and deposition by interaction with CO and O_2

To evaluate the reducibility of the fully oxidized supported RuO_2 NPs we sent a sequence of CO/Ar (1:1) pulses (Δt = 20 s) over the oxidatively pretreated (O150) Ru/Al_2O_3 catalyst at 190 °C. Previous surface science type experiments indicated that CO can efficiently react with RuO_2(110) already at temperatures below room temperature [47,48], and we expect the same also for RuO_x nanoparticles for reaction at 190 °C.

The number of gas pulses was chosen such that at the end of the sequence there were only insignificant changes in the signal height, which in this case was reached after 540 CO pulses in total. Fig. 1a shows the integrated mass spectrometric signals of the first 360 CO pulses during CO/Ar pulsing, integrated for each pulse over the time of a pulse. The full sequence is shown in Fig. S1 in the Supporting Material. As mentioned in chapter 2.2, the start of a new sub-sequence of pulses, i.e., after 180 pulses (Fig. 1) and 360 (Fig. S1), led to significantly smaller pulses, which recovered, however, after a few pulses. During the first approx. 260 pulses, the CO signal was rather low, indicating almost complete consumption of CO. Then the pulse size increased sharply, until in the last approx. 150 pulses the increase was rather slow (see Fig. S1). The pulses of CO_2, which were formed upon interaction of the pulsed CO with the pre-oxidized catalyst in the same sequence, are presented in Fig. 1b. In the beginning, the CO_2 signal area was high, as expected for an almost complete consumption of CO (Fig. 1a). After approx. 260 pulses it decreased strongly, but even at the end of the sequence the CO_2 signal had not reached the background level. Note that more pronounced decay in the CO_2 signal intensity at the beginning of a new sub-sequence is due to the considerable broadening of the effluent CO_2 pulses, caused by the rather strong interaction between CO_2 and the catalyst surface. As a result, it takes about 10 pulses of CO_2 after the end of the first break, at the beginning of the second pulse sequence, before the CO_2 signal again reaches its previous height (see Fig. S2). The trend of the decreasing CO_2 intensity agrees very well with expectations based on the decreasing consumption of CO. Hence, the time-dependent consumption of CO is qualitatively correlated with the formation of CO_2. The formation of CO_2 together with the removal of CO confirms the reaction of the pulsed CO with the RuO_2 NPs. However, we cannot exclude that oxidic Ru species may remain at least in the inner part of the NPs.

After the reduction by CO pulses, we subsequently re-oxidized the catalyst by 540 pulses O_2/Ar (1:1) at 190 °C (Δt = 20 s). Also this sequence was separated into three sub-sequences of 180 pulses each.

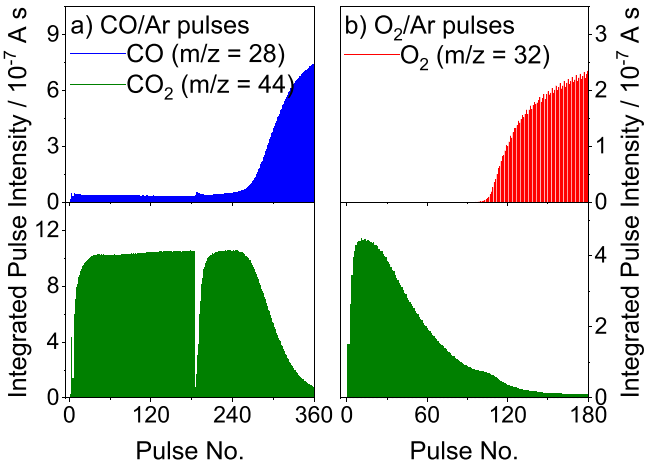

Fig. 1. Integrated intensities of a) the first 360 pulses in a sequence of CO/Ar pulses at 190 °C after O150 pretreatment of Ru/Al_2O_3 (blue: CO, green: CO_2), and b) of the first 180 pulses of a subsequent sequence of O_2/Ar pulses at 190 °C (red: O_2, green: CO_2).

The integrated O_2 pulse signals of the first 180 pulses are plotted in Fig. 1c. In the first 100 pulses the signals were close to the background value, indicating complete consumption of pulsed O_2. Then the signals increased steeply, until after approx. 200 pulses this increase became smaller again, and the O_2 pulses approached an almost constant level (see Fig. S1c). Interestingly, also O_2 pulsing led to the formation of CO_2. The CO_2 pulses in this sequence, which are shown in Fig. 1d, were highest in the beginning of the sequence and then decreased almost exponentially to reach the background level after about 180 pulses. The amount of CO_2 released during O_2 pulsing is, however, much less than that obtained during CO pulsing. Furthermore, in contrast to the CO/Ar sequence, where the increase in CO_2 signal and decrease in CO_2 signal occurred simultaneously, these signals seem to be decoupled in the subsequent O_2 pulse sequence, as the CO_2 signal appears only in the initial phase of O_2 pulsing and decays long before the increase in the O_2 pulse intensity. Most simply, the formation of CO_2 during O_2 pulsing can be explained by an O_2-induced decomposition of surface carbonate species [49,50], which were formed during CO pulsing, due to reaction of CO_2 resulting from the titration with active surface oxygen present on the catalyst surface. This will be discussed further below. During CO pulsing, in contrast, the observed CO_2 product was mainly formed from the interaction of CO in the CO/Ar pulses with active surface oxygen species, which are present on the surface as a result of the O150 pretreatment.

The trends in the pulse intensities of the consumed species, CO or O_2, and of the reaction product CO_2 are comparable to the ones previously observed in similar titration experiments of active oxygen on Au/TiO_2, [51], on nanoporous gold (NPG) [52], or on Au/ZnO [53]. These previous cases differ, however, in that for Au/TiO_2 and for NPG the consumption of CO became negligible at the end of the pulse sequence. In contrast, for the latter system we could show that there was a small but continuous consumption of CO also at later stages, when the CO pulse intensity remained constant. This ongoing consumption of CO and formation of CO_2 was attributed to a continuous segregation of oxygen to the partly reduced interface perimeter sites of ZnO [53,54]. For the present experiments and reaction conditions we exclude surface reduction of the Al_2O_3 support and segregation of oxygen. On the other hand, the formation of surface carbonate species, which we had proposed above, could result in continuous CO consumption without measurable CO_2 formation.

The possibility of carbonate formation was tested directly by XPS measurements of a catalyst that after an O150 pretreatment was exposed to a sequence of 1000 CO pulses. Subsequently, the sample was removed from the micro-reactor in a glove box, to exclude contact to air, mounted on a sample holder and then transferred to the XPS set-up in a transfer vessel, thereafter it was introduced into the XPS chamber also without contact to air. For comparison, we preformed similar experiments also directly after O150 pre-treatment and after exposing an O150 pretreated catalyst to 1000 pulses of CO_2/Ar. Overview spectra and detail spectra of the C 1s / Ru 3d region of the three measurements are shown in Fig. S5. The XPS measurements after CO pulsing resolved a C 1s peak at 288.9 eV (Fig. S5a), which can be assigned to the presence of surface carbonates [45]. A quantitative analysis of the carbonate C 1s and the Ru $3d_{5/2}$ peak intensities revealed comparable amount of surface carbonate after CO and CO_2 pulsing, while it was significantly lower directly after O150 treatment (for details see the Supporting Material). Hence, the XPS results are fully consistent with the formation of significant amounts of surface carbonate species on the pre-oxidized catalyst surface during CO pulsing, supporting our conclusions derived from the mass balance in the pulse sequences. Furthermore, the similar amounts of carbonate formed during CO and CO_2 pulsing indicate that this is not limited by the amount of CO_2 molecules, which is different during CO_2 pulsing and during CO pulsing, since CO is only partly converted into CO_2. Instead, it seems to be limited by the availability of specific reaction sites on the catalyst surface.

Similar titration experiments to the ones described above were performed also at 250 °C and 300 °C, the resulting sequences of integrated pulse intensities are presented in Figs. S3 and S4, respectively. Because of the more pronounced reaction, four sub-sequences with 720 pulses in total were necessary to approach steady-state conditions at these higher temperatures. Main results of these measurements are that in both cases the CO pulse area was rather low in the beginning of the sequence, and then increased steeply to finally reach a constant pulse size. For CO pulsing at 250 °C (Fig. S3), the steep increase started also at about 260 pulses and constant pulse size was reached after about 450 pulses. Compared to reaction at 190 °C, the increase of the CO signal essentially occurred after the same number of pulses, and this is true also for CO pulsing at 300 °C. In total, there are no big temperature effects in the CO pulse characteristics. Focusing on the CO_2 signal, this remained initially at a high constant value, and started to decrease after about 250 pulses, i.e., at the same point where the CO consumption decreased. This is followed by an about exponential decay, reaching the background level at the end of the sequence, after about 700 pulses, which is close to the result obtained during CO pulsing at 190 °C. For CO pulsing at 300 °C (Fig. S4), the general trends are identical with those at 250 °C, with the only difference that the CO_2 pulse intensity was higher in the later stages of the CO pulse sequence (Fig. S4b), indicative of ongoing CO_2 formation. This would fit also to the observation that the CO pulse size increased slightly in that part of the pulse sequence. In total, these data indicate a complex temperature dependence that will be discussed in more detail later after the presentation and discussion of the O_2-pulse data and the accumulated gas consumption.

In the subsequent O_2 pulse sequence the O_2 signal size (Fig. S3c) was rather low in the first approx. 200 pulses, then increased quickly and finally changed to a slower increase at about 300 pulses. In the end of the sequence, an almost constant O_2 pulse size was reached. The corresponding CO_2 signal (Fig. S3d) increased steeply in the first few pulses, to reach a maximum after 5 pulses, and then decreased exponentially. In general, these trends are comparable to those at 190 °C, with the only difference that at 250 °C, the increase in the O_2 signal as well as decline in CO_2 signal is slower and starts later compared to the data obtained at 190 °C. For O_2 pulsing at 300 °C (900 pulses), the phase of complete O_2 consumption was even longer and the O_2 pulse size increased only after about 500 pulses, in a similar way as observed before at 250 °C, but with the difference that even after 900 pulses the increase in pulse size was significant. Obviously, O_2 consumption was much more pronounced under these conditions. Also for the CO_2 signal (Fig. S4d), the trend is comparable to that at 250 °C, with a steep increase in the initial few pulses, followed by a continuous decay, which neglecting the breaks in intensity is also about exponential. Similar to the behavior in the CO sequence, we still find some CO_2 formation at the end of the sequence, indicating ongoing O_2 consumption and CO_2 formation also in this stage.

For more quantitative information we evaluated the accumulated number of active oxygen species removed and deposited during CO pulsing and O_2 pulsing, respectively. Fig. 2a - c shows the accumulated CO conversion (O_{act} depletion) per g catalyst in a sequence of CO/Ar pulses after O150 on the $Ru/\gamma - Al_2O_3$ catalyst at different reaction temperatures of 190 °C, 250 °C, and 300 °C (see pulse sequences in Fig. 1a, Fig. S3a and Fig. S4a).

The accumulated oxygen consumption in the subsequent O_2/Ar pulse sequence is shown in Fig. 2d-f for the different reaction temperatures of 190 °C, 250 °C, and 300 °C. At 190 °C and 250 °C, the O_2 consumption after 540 pulses was rather small and constant, while for the measurement at 300 °C even after 900 pulses there was measurable O_2 consumption (for the corresponding pulse sequences see Figs. S3 and S4). At all temperatures the O_{act} deposition is initially identical, at least during the first 150 pulses, due to complete consumption of the O_2 pulses in this range (phase I), while at later stages (phase II) it is lower. Different from the CO consumption, however, the transition from phase I to phase II shifts to higher pulse numbers with increasing temperature, from about 120 pulses at 190 °C to about 600 pulses for deposition at 300 °C. In contrast, for CO pulsing this was always at about 300 pulses.

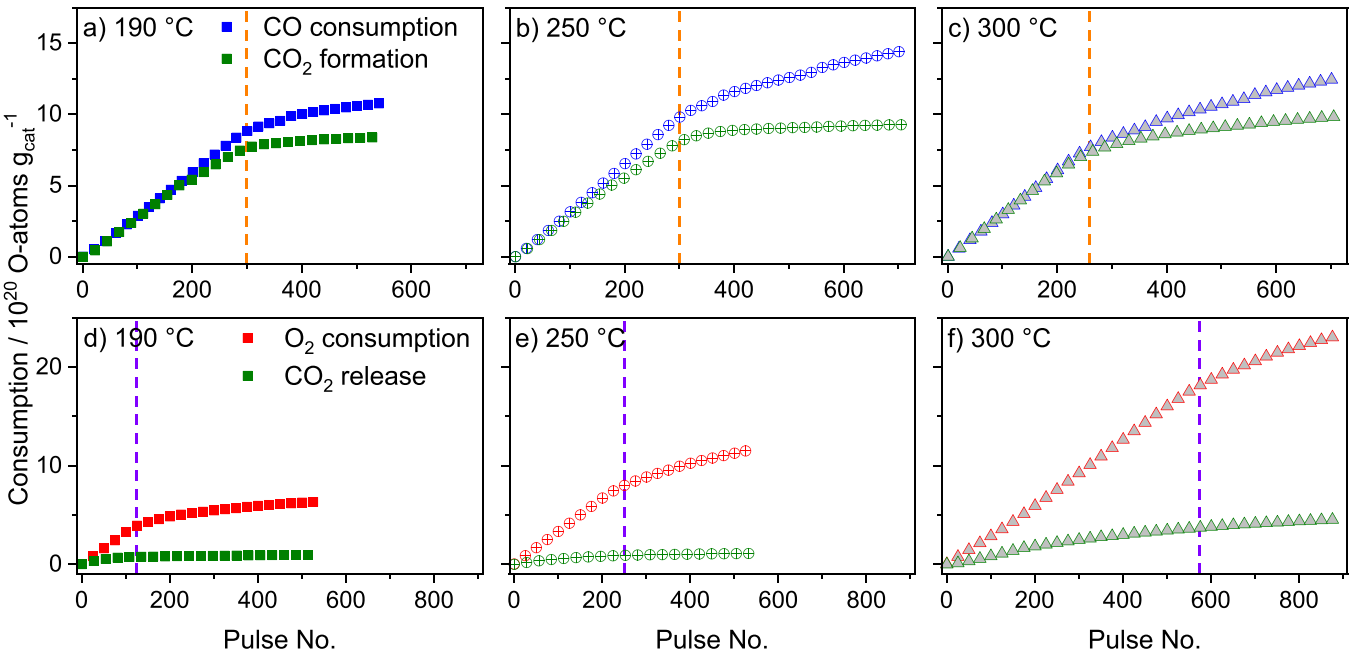

Fig. 2. Accumulated CO consumption and CO_2 formation in a CO/Ar pulse sequence (a-c) and O_{act} replenishment as well as CO_2 formation in a subsequent sequence of O_2/Ar pulses (d-f) on a Ru/Al_2O_3 catalyst, after O150 pretreatment, at the different temperatures indicated. The dashed lines indicate the transition from phase I (higher slope) to phase II (lower slope).

Furthermore, also the ongoing O_2 consumption in phase II increased with increasing temperature, as evidenced by the higher final slopes. Overall, the temperature dependence of the oxygen replenishment was more pronounced than that for oxygen removal (CO consumption). Most simply this can be explained by an ongoing oxidation of carbon-containing adsorbate species already present on the catalyst, which is more efficient at higher temperatures.

The total numbers for the accumulated CO consumption and CO_2 formation during CO pulsing, and for O_2 consumption and CO_2 release in the following sequence of O_2/Ar pulsing are summarized in Table 1 for the different temperatures. Therein, we distinguish also between the initial phase with higher slope (phase I) and the later phase with lower slope (phase II). Considering that each CO molecule is able to remove one oxygen atom from the catalyst surface, the amount of CO consumption in molecules per g catalyst equals the number of oxygen atoms removed per g catalyst. Similarly, we assume that each O_2 molecule can deposit two O atoms. Already at 190 °C, the CO consumption of 1.08×10^{21} molecules g_{cat}^{-1} corresponds to a removal of 3.6 active oxygen atoms per Ru atom, where the latter value was obtained by normalizing the amount of CO consumed per g catalyst to the total number of Ru atoms present on the catalyst, which was given by the Ru loading of the catalyst (5 wt%). This is well above the amount of oxygen that can be removed from completely oxidized RuO_2 NPs, during reduction to Ru NPs. The discrepancy to the stoichiometry of the stable RuO_2 phase may partly be due to O_2 adsorption, but in any case, we can assume that the Ru NPs were completely oxidized to RuO_2 during the O150 pretreatment, which is consistent also with previous findings for a comparable catalyst [37]. The observation of significantly less CO_2 formation as compared to CO consumption can simply be explained by the build-up of surface carbonates, due to reaction of CO_2 with the support. This CO_2 formed by reaction of CO with O_{act} species can further react with surface oxygen on the support, either directly at the interface, or by spill-over of adsorbed CO_2 to the Al_2O_3 support, or after desorption and subsequent re-adsorption. This second step agrees with conclusions in previous studies, which reported surface carbonate formation on γ-Al_2O_3 surfaces upon interaction with CO_2 [55,56].

The third interesting result is that although O replenishment seems to be very efficient, the total amount of replenished O is still less than the O removal, even when using the value of CO_2 formation rather than that for CO consumption. Most likely, this apparent lack of reversibility is caused by kinetic limitations in the re-oxidation of the reduced Ru particles at lower temperatures (190 °C and 250 °C) (see Table 1). In contrast, at 300 °C, the data seem to indicate even a strong excess in oxygen re-deposition, which we tentatively attribute to the oxidation of carbon containing surface contaminations at these high temperatures, which were not oxidized during the O150 pretreatment. This would explain also the considerable amount of CO_2 formation in the O_2 pulse sequence at this temperature.

In addition to the CO and O_2 consumption, we quantified the formation of CO_2 from CO pulsing in this sequence from the CO_2 pulse intensity. At all reaction temperatures, the difference between CO consumption and CO_2 release is negligible in the first phase, in the regime of complete CO consumption. In contrast, after that phase, less CO_2 was released from the catalyst bed than CO consumed, and this discrepancy

Table 1
Resulting CO consumption and CO_2 formation in CO/Ar pulses after O150 and O_2 consumption / CO_2 formation during subsequent O_2/Ar pulses on Ru/Al_2O_3 at different reaction temperatures separated for the initial phase with higher slope (phase I) and the later phase with lower slope (phase II).

		CO/Ar pulses		O_2/Ar pulses	
T / °C		CO consumed /10^{20} O atoms g_{cat}^{-1}	CO_2 formed /10^{20} molecules g_{cat}^{-1}	O_2 consumed /10^{20} O atoms g_{cat}^{-1}	CO_2 released /10^{20} molecules g_{cat}^{-1}
190	Phase I	8.8	7.6	3.9	0.76
	Phase II	2.0	0.8	2.5	0.19
250	Phase I	9.8	8.1	8	0.9
	Phase II	4.7	1.2	3.4	0.2
300	Phase I	7.7	7.3	18.1	3.7
	Phase II	4.9	2.6	5.2	0.9

varied with temperature. While the difference increases from 190 °C to 250 °C, it decreases again at 300 °C. Furthermore, also the CO consumption increases at 250 °C and is lower again at 300 °C. We tentatively assign these trends to a combination of temperature enhanced carbonate formation and increasing carbonate decomposition, where the first effect is dominant from 190° to 250°C, while the latter one is responsible for the increasing CO_2 release in phase II at 300 °C.

For more information on the nature and stability of the adspecies formed during CO/Ar pulsing, we performed a temperature programmed desorption (TPD) measurement after the CO/Ar sequence at 190 °C. In this measurement, the catalyst was heated from the reaction temperature of 190 °C to 450 °C. This temperature was held for 5 min, then the catalyst was cooled down to 190 °C again. Both heating as well as cooling rate were 25 °C·min^{-1}. The T-dependent desorption rates of the respective species, which were calculated from the mass spectrometric signal and the specific sensitivity, are presented in Fig. 3. The detected signal intensities in this experiment are presented in Fig. S6 and summarized in Table S1.

In the TPD after CO/Ar pulsing, there was only background signal for O_2 (not shown). A small amount of water desorbed from the catalyst with a peak temperature of 314 °C. Since during pulsing there was no H_2 dosed to the catalyst, water must have been present on the catalyst surface before the pulse experiment, e.g., due to exposure to air, and was not completely removed during the pretreatment or pulsing. CO desorbed with a shoulder at 325 °C and then continued to evolve up to the maximum temperature, where desorption started to decrease again. Considering the adsorption energy of CO on Ru, most of the CO evolution must result from the decomposition of adsorbed species which were formed during CO pulsing, such as surface carbonates. In contrast, at 190 °C, desorption of adsorbed CO should occur instantaneously after finishing the CO pulse sequence, which is supported also by the negligible CO intensity at the onset of the TPD run. Main desorption product in this measurement was CO_2, which desorbed with two peaks at 276 °C and 407 °C. (Note that the decay of the signal at 407 °C cannot be due to the end of the heating period, as this stopped only at 450 °C.) Also, these peaks must result from decomposition of stable adsorbed species such as carbonates. The existence of two separate peaks indicates that at least two different types of such species were present on the catalyst surface. This finding supports our previous idea that a carbonate adlayer was formed during CO pulsing, which was based on the discrepancy between CO consumption and CO_2 formation.

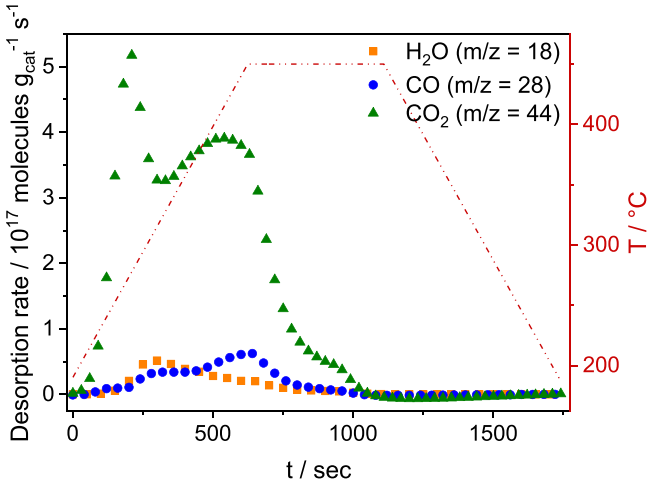

Fig. 3. Desorption rate of H_2O (yellow), CO (blue), and CO_2 (green) in a TPD experiment from a Ru/Al_2O_3 catalyst after O150 pretreatment and subsequent exposure to 1000 CO/Ar pulses. The catalyst was heated from the reaction temperature of 190 °C to 450 °C (r = 25 °C•min^{-1}), and cooled down after 5 min to 190 °C (r = 25 °C•min^{-1}), as indicated by the red dashed temperature profile.

From the difference between CO consumption and CO_2 release during CO pulsing (see Table 1), we estimated the amount of carbonate species generated on the catalyst surface to be 2.4×10^{20} molecules g_{cat}^{-1} or 2.4×10^{14} carbonate species per cm_{cat}^{2}. In the TPD experiment, the accumulated amount of CO_2 desorption was 2.1×10^{20} molecules g_{cat}^{-1}, which was almost the amount of carbonate build-up during CO pulsing derived from Fig. 1a and b. Since in the first 300 pulses of the CO/Ar sequence almost the same amount of CO_2 was formed as CO consumed per pulse, we expect the carbonate build-up to start after approx. 300 pulses, when the catalyst was already in a mainly reduced state.

For comparison, we also performed a similar TAP-TPD experiments with a catalyst that was exposed to 1000 pulses CO_2/Ar subsequent to O150 pretreatment, where based on literature reports on the interaction of Al_2O_3 with CO_2 we expect the formation of surface carbonates (Fig. S7, Table S2). In this TPD measurement we found a comparable amount of CO_2 desorbing from the catalyst surface, and the TPD profile resembles that obtained after CO pulsing other also in the peak positions, with a pre-peak (CO/Ar) or a shoulder at about 275 °C and a main peak at about 415 °C or 450 °C, respectively. There are, however, differences in the relative intensities of these features after CO/Ar pulsing and after CO_2/Ar pulsing, with a more pronounced pre-peak after CO/Ar pulsing. Furthermore, after CO_2 pulsing desorption in the main peak increases up to the maximum temperature, which may indicate that there are additional, more stable species on the surface whose decomposition may lead to CO_2 formation and desorption as well. As a result, the number of surface species producing CO_2 upon thermal decomposition (desorption of adsorbed CO_2 can be ruled out at these desorption temperatures) seems to be somewhat higher after CO_2 pulsing than after CO pulsing (see Tables S1 and S2), which would be compatible with the XPS results. The general nature of these surface species, however, seems to be similar in both cases, as evidenced by the desorption peak temperatures. Since carbonate formation is well-known for Al_2O_3 support upon exposure to CO_2 [57,58], this supports our previous conclusions that exposure of the O150 pre-oxidized catalyst to CO/Ar pulses leads to surface carbonate formation. For the O150 pretreated catalyst, in contrast, the amount of these surface species is drastically lower (see Table S3), supporting that these species are formed during exposure to CO or CO_2 pulses. Finally, the much higher amount of these surface species on the fresh catalyst (see Table S3) can be explained by the long exposure of the raw catalyst to CO_2 from the atmosphere.

The formation of carbonate adspecies on a reductively pretreated Ru/Al_2O_3 catalyst in a CO_2 stream was detected also by diffuse reflectance infrared Fourier transform spectroscopy (DRIFTS) - mass spectrometry (MS) measurements by Wang et al. [59] and in DRIFTS measurements by Dongapure et al. [60]. These authors concluded that the carbonate species were formed by interaction of CO_2 with hydroxyl groups on the Al_2O_3 surface, which had also been observed on bare γ-Al_2O_3 [58,61]. Weilach et al. suggested that i) CO can react with OH groups on Al_2O_3 to form CO2 and that ii) CO_2 reacts subsequently either with coordinatively unsaturated (cus) O^{2-} ions of Al_2O_3 or inserts into oxygen vacancies to form monodentate or bidentate carbonate species, respectively [57].

In this part, we showed that the CO pulses essentially reduce the RuO_2 NPs at all temperatures investigated. This resulted in the formation of CO_2, which was released from the catalyst bed. From the differences in CO consumption and CO_2 formation we concluded on the formation of surface carbonates that remained on the Al_2O_3 support. In the subsequent O_2 pulse sequences O_{act} was replenished on the Ru NPs. Here the O_2 consumption was lower than that of CO in the preceding sequence at 190 °C and 250 °C, but higher at 300 °C. Furthermore, part of the surface carbonates formed during CO pulsing were decomposed by interaction with O_2, resulting in CO_2 release.

3.2. *Active oxygen deposition by interaction with CO_2*

Next, we studied the ability of CO_2 to replenish active oxygen on the

catalyst compared to O_2. Similar to the procedure for CO / O_2 pulsing, we first exposed the catalyst to the oxidative treatment (O150), followed by a sequence of 540 CO/Ar pulses to reduce the oxidized Ru NPs. Afterwards, we sent a sequence of 720 pulses CO_2/Ar (molecular ratio 1:2) ($\Delta t = 20$ s) over the catalyst. In similar experiments, CO or H_2 was added to the CO_2/Ar gas mixture (molecular ratio 1:1:1), respectively, to evaluate the ability of CO_2 to re-oxidize the Ru NPs in the presence of a reducing agent, which mimicked the realistic CO_2 reduction reaction conditions. The integrated pulse intensities of CO_2 and of the respective added reducing agents, CO or H_2, are shown in Fig. 4 for the first 150 pulses of each measurement. The full sequences are shown in Fig. S9. The CO_2 signal in the CO_2/Ar pulses (Fig. 4a) was significant already in the first pulse and then increased slightly, until reaching a maximum after about 25–30 pulses. Subsequently, it decreased again until reaching an about stable state after about 150 pulses. Possible reasons for this apparent decay will be discussed later in Section 3.3. The resulting trend is very different from that observed during O_2 pulsing (Fig. 1c), where we observed complete O_2 consumption in the first 100 pulses. Hence, the reactivity for CO_2 consumption, by re-oxidation of the reduced catalyst (O_{act} formation) and formation of CO (Fig. 4a), is much less than that for oxidation by O_2 pulses. The resulting CO is indeed detected, supporting this idea.

Comparing the measured intensity of the effluent CO_2 pulses with that of the incoming CO_2 pulses, which is almost identical to the Ar pulses indicated by the black dotted line in Fig. 4a, it looks like that there is an excess of CO_2 formation, i.e., there is more CO_2 leaving the catalyst bed than initially present in the pulses, before interaction with the catalyst bed. The intensity of the incoming CO_2 pulses and the number of CO_2 molecules therein was calculated from the measured Ar signal intensity in the CO_2/Ar pulses and the known CO_2 : Ar ratio in the pulses. This surprising result will be discussed in more detail later with the isotope labelling experiments in Section 3.3.

In Fig. 4b we show the CO and CO_2 signals in the CO/CO_2/Ar pulse sequence. Note that the number of CO_2 molecules per pulse was identical in all of these sequences (for the number of pulses see Fig. S9). In this case we find rather stable CO_2 pulse sizes over the whole sequence of 540 pulses, except for the initial increase as described above. The CO signal also increases initially, reaching its maximum already after a few pulses. Subsequently it decays slightly. We note that different from Fig. 4a the CO signal in Fig. 4b is a combination of a small amount of CO formation and the much larger CO component in the gas mixture. The formation of additional CO, in addition to that present in the reactant gas, could be verified by comparing the intensity of the CO pulses with the Ar intensity, considering that the gas composition was fixed (CO : CO_2 : Ar = 1:1:1). Also in this case we find an excess of CO_2 in the pulses after interaction with the catalyst. However, it is much more pronounced in the CO/CO_2 mixture than in Fig. 4a. Here, at least part of the additional CO_2 intensity can be explained by oxidation of the CO in the mixed CO/CO_2 pulses, by reaction with O_{act} that had been deposited by interaction of the surface with CO_2 before. But also when comparing the amount of pulsed CO and CO_2 molecules, which can be determined by comparison with the Ar signal, with the number of detected CO_2 molecules, we find an excess of CO_2 molecules in the detected pulses. This supports our previous conclusion that there must be a carbon source on the catalyst surface, which can contribute to the CO_2 release, in addition to the molecules resulting directly from the CO/CO_2 pulses.

Finally, in the sequence of H_2/CO_2/Ar pulses, the CO_2 pulse size was again constant over the whole sequence, except for the initial increase (Fig. 4c). This is similar to the trends in the other gas mixtures. Its absolute intensity is, however, only half of that obtained during CO_2/Ar and CO/CO_2/Ar pulsing. There is again an excess of CO_2, but both the absolute intensity of the CO_2 pulses as well as the CO_2 excess are approximately identical to those in Fig. 4a. The CO signal, which in this case can either result from the decomposition of $CO_{2,ad}$ or from the reverse water-gas shift reaction between CO_2 or formate species and H_2, essentially follows the CO_2 signal (Fig. 4c). Furthermore, it is slightly higher than that in Fig. 4a, supporting the existence of an additional pathway for CO formation. The H_2 signals finally were too low for a reliable integration. H_2 can, in addition to reacting with O_{act} from the Ru surface, also react with adsorbed CO_2 or formate adspecies to form CH_4 and H_2O [62]. The continuous formation of small amounts of CH_4 during CO_2/H_2 pulses was indeed confirmed by the mass-spectrometric signal (see pulse signals in Fig. S10).

A closer look at the carbon balance between incoming CO and CO_2 pulses on the one hand detected CO, CO_2 and CH_4 pulses on the other hand (see Table S4) reveals that there is a considerable deficit in the

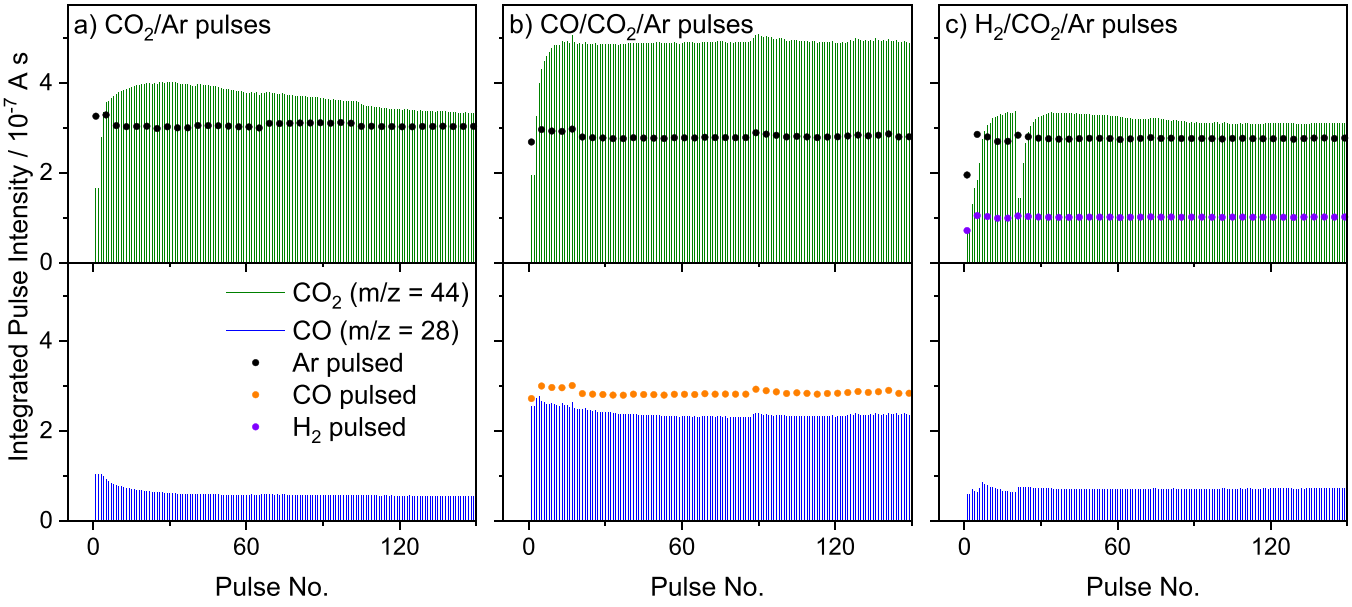

Fig. 4. Integrated intensities of a) CO_2 (green) and CO (blue) pulses during the first 150 pulses of CO_2/Ar (1:2) after O150 and CO/Ar pulsing on Ru/Al_2O_3 at 190 °C. b) and c) similar signals during the first 150 CO/CO_2/Ar (1:1:1) pulses and 150 H_2/CO_2/Ar (1:1:1) pulses, respectively, all after O150 and 540 CO/Ar pulses. The dotted lines indicate the detected Ar (black), CO (yellow, Fig. 4b) and H_2 (blue, Fig. 4c) signals, respectively. The size of the CO_2 pulses is essentially identical to that of the Ar pulses (96.1% of the Ar pulses). The complete pulse sequences of these experiments are presented in Fig. S9. For the H_2/CO_2/Ar pulse sequence we show a version including also the CH_4 product pulses in Fig. S10.

carbon balance, when only considering the incoming CO_2 pulses and the effluent CO, CO_2 and CH_4 pulses. We suggest that this deficit is balanced by the decomposition of surface carbonate species during CO_2/H_2 pulsing, which had been present on the surface at the beginning of the CO_2/H_2 pulse sequence, i.e., after O150 pretreatment and subsequent reduction by CO pulses. In fact, the deficit in the carbon balance (2.9×10^{20} atoms g_{cat}^{-1}, see Table S4) is very close to the amount of carbonate formation calculated for exposure of the O150 pre-treated catalyst to CO pulses in the experiment described in Fig. 1 (2.4×10^{20} atoms g_{cat}^{-1}, see Table S4), which fully supports our explanation.

To clarify the question whether CO_2 pulsing leads to O-deposition, which could not be resolved directly from the CO_2 pulses, we tried to determine the amount of active oxygen deposition by subsequent CO pulsing at 190 °C, assuming that the consumption of CO in this sequence corresponds to the total amount of O_{act} deposited before by CO_2. The accumulated consumption of CO corresponding to the active oxygen replenishment by CO_2 in the preceding sequence is shown in Fig. 5. Similar experiments were performed subsequent to the oxygen deposition in pulses of $CO/CO_2/Ar$ and $H_2/CO_2/Ar$ gas mixtures. For better comparison we also show the value obtained from the re-oxidation measurement with O_2/Ar pulses (Fig. 2b). The signal intensities of the related CO/Ar pulse sequences employed to titrate O_{act} from the catalyst are shown in Figs. S11–S13, respectively. Based on these results, 540 pulses of pure CO_2/Ar pulses could deposit 58% of the active oxygen deposited from O_2 in the pulses at 190 °C on Ru/Al_2O_3 (Fig. 1c).

In the presence of CO, in $CO/CO_2/Ar$ pulses, the amount of O_{act} deposited on the catalyst was lower than when pulsing CO_2/Ar, with 41% of that deposited in O_2/Ar pulses. As expected, the presence of the additional reduction agent CO results in partial removal of the O_{act} deposited from CO_2. Considering that in this scenario CO_2 was consumed and formed at the same time, the actual CO_2 consumption could not be calculated from the CO_2 signal, only the combination of both processes is accessible as an effective O_{act} deposition.

Interestingly, in the presence of H_2 in the gas mixture, CO_2 was able to deposit a comparable amount of active oxygen on the catalyst as when pulsing O_2/Ar. Most simply, the enhanced deposition of O_{act} can be explained by the formation of highly reactive water via the reverse water-gas shift (RWGS) reaction under these conditions. The reaction of CO_2 with H_2 may also lead to the formation of CH_4 under these conditions. Compared to the total O_{act} deposition, as determined by subsequent CO pulse titration, approx. 7% of the consumed CO_2 molecules were converted to CH_4. The observation of both CO and methane formation would be consistent with the possible formation of a CO_2 hydrogenation product on the surface, such as adsorbed formates, that can either be hydrogenated to methane or decompose to form CO (RWGS) [24,39]. The observation of methane formation in the pulse experiments finally indicates that despite the pressure gap compared to realistic reaction conditions, the results of these experiments are relevant also for the reaction behavior under realistic reaction conditions.

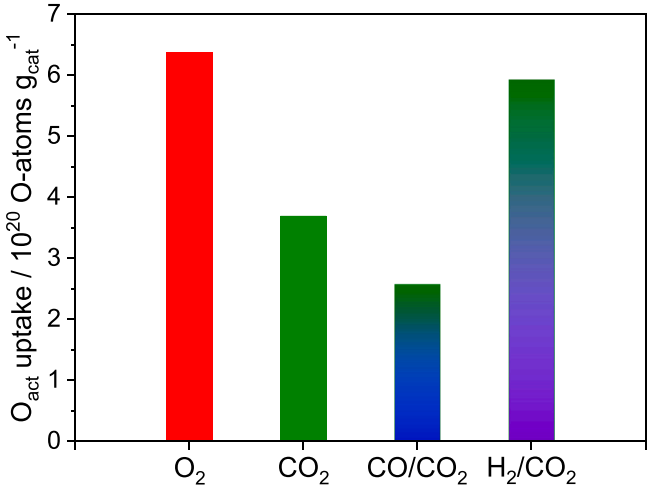

Fig. 5. Amount of active oxygen replenished in a sequence of O_2/Ar pulses (red), CO_2/Ar pulses (green), $CO/CO_2/Ar$ pulses (blue/green), and $H_2/CO_2/Ar$ pulses (purple/green) sent at 190 °C on a pre-reduced Ru/Al_2O_3 catalyst, each determined by 360 CO/Ar pulses.

In total, we have shown that CO_2 is able to deposit O_{act} on the pre-reduced Ru/Al_2O_3 catalyst. It is, however, considerably less active than O_2. If CO is additionally present in the pulsed gas this can remove part of the freshly replenished O_{act} from the catalyst again, while addition of H_2 leads to an increase of the O_{act} deposition activity. The latter reaction most likely involves the formation of highly reactive water (reverse water gas shift reaction) and its subsequent reaction with the surface.

3.3. Reversible oxygen exchange during interaction with CO_2

Finally, for an unambiguous interpretation of the above results on the interaction of CO_2 with the catalyst surface, we performed an isotope labelling experiment, pulsing isotope labelled $C^{18}O_2$ on an O150 pre-treated and subsequently reduced (CO/Ar pulses) Ru/Al_2O_3 catalyst. During $C^{18}O_2$ pulsing we expect to observe i) the deposition of labelled active oxygen ($^{18}O_{act}$) on the surface of the reduced catalyst (comparable to the measurements shown in Fig. 4a) and ii) possibly the release of species resulting from the interaction of CO_2 with adsorbed species present on the surface, e.g., due to isotope exchange. The evolution of the integrated intensity of the $C^{18}O$ pulses during a sequence of 900 pulses at 190 °C is illustrated in Fig. 6a. As in previous measurements, the experiment was performed in five consecutive sub-sequences, which are indicated by the lower intensity pulses at the beginning of each subsequence. The pulse area of the $C^{18}O_2$ signal (Fig. 6a) increased steadily in the first 360 pulses, then the increase became slower and at the end of the sequence the $C^{18}O_2$ pulse size seems to approach a constant value. This is very different from the observation in Fig. 4a, which describes the trends during a similar experiment, but using $C^{16}O_2$ pulses. In that case the CO_2 pulse intensity had quickly reached its maximum value, followed by a slow decrease. Using the Ar pulse sizes for calibration, this seems to be a real effect. Most simply, this difference between $C^{16}O_2$ consumption (Fig. 4a) and $C^{18}O_2$ consumption (Fig. 6a) results from the reactive formation of the other isotopomers, $C^{18}O^{16}O$ and $C^{16}O_2$. Those could not be identified in the earlier experiment with $C^{16}O_2$ pulses as CO_2 consumption, but rather appeared as 'non-consumed CO_2'. We indeed find significant formation of $C^{16}O^{18}O$ and $C^{16}O_2$ pulses (Fig. S14), meaning that there is significant reactive interaction between CO_2 and the reduced catalyst or adsorbed species present on this catalyst also for longer times. This, however, mainly leads to CO_2 products and is therefore visible only in isotope labelling experiments. In Fig. S14a we also indicate the intensity of the incoming $C^{18}O_2$ pulses, as derived from the Ar pulse intensity and the known $C^{18}O_2$: Ar ratio in the pulses. It already indicates, that at the end of the sequence almost all $C^{18}O_2$ is passed through the catalyst bed without being consumed, which means that measurable formation of the other isotopomers would result in an excess of CO_2 emission during CO_2 pulses.

For the $C^{16}O^{18}O$ signal, which indicates partial oxygen exchange between catalyst and $C^{18}O_2$, we find a steep initial increase of the pulse intensity (Fig. S14b). It then bends off, passes through a maximum at approx. 160 pulses, and subsequently declines linearly. In the end of the sequence, there is still a significant $C^{16}O^{18}O$ signal detected. For $C^{16}O_2$ (Fig. S14c), reflecting complete oxygen exchange between catalyst, and $C^{18}O_2$, we observe an even steeper initial increase, a maximum at about 10 pulses, and subsequently an exponential decay. Finally, we also detected some $C^{16}O$ formation (Fig. S14d). The CO signal was, however, small and rather stable during the whole sequence.

Combining the signals of all three CO_2 isotopomers, we obtain the pulse signals shown in Fig. S14e, where the different colors indicate the

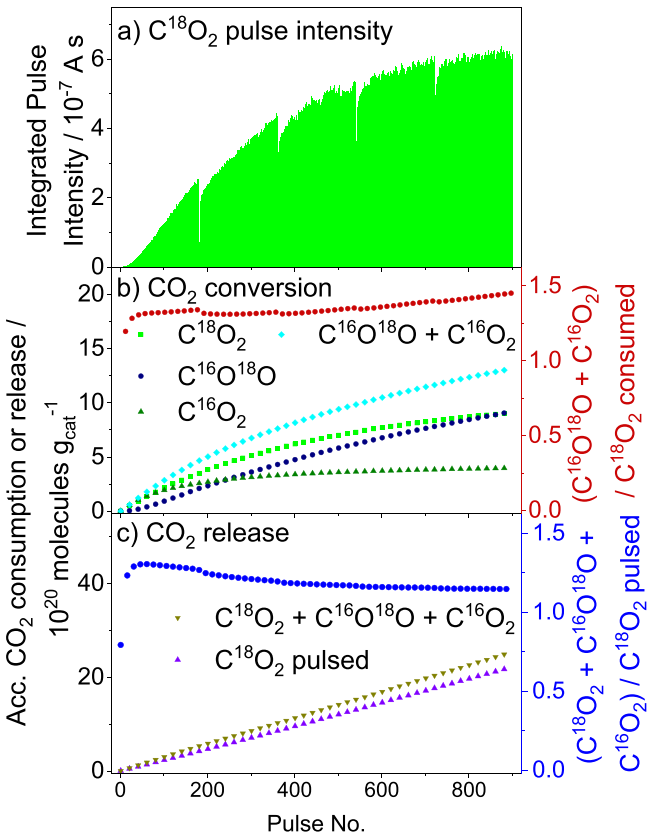

Fig. 6. a) Integrated $C^{18}O_2$ intensity in $C^{18}O_2$/Ar pulses at 190 °C after O150 and CO/Ar pulse reduction. b) Resulting accumulated net $C^{18}O_2$ consumption (bright green), $C^{16}O^{18}O$ formation (dark blue), $C^{16}O_2$ formation (dark green), as well as the sum of $C^{16}O^{18}$ and $C^{16}O_2$ formation (turquoise) in that pulse sequence. The relative amount of $C^{16}O^{18}$ and $C^{16}O_2$ formation compared to the $C^{18}O_2$ consumption (see Fig. S14a) is indicated by the brown dotted line. c) Accumulated amount of incoming $C^{18}O_2$ molecules (purple) and of the three different CO_2 isotopomers detected in the pulses formed (olive). The relative amount of excess CO_2 formation, the ratio of outgoing to incoming CO_2 molecules is indicated by the blue dotted line.

contributions of the different isotopomers. The general trend closely resembles that in Fig. 4a, with a steep increase in the initial phase, during the first few pulses, followed by a slight decrease and then an about constant intensity These data clearly indicate that CO_2 pulsing leads to an excess of CO_2 emission, i.e., more CO_2 is emitted than contained in the incoming pulses, fully supporting our initial conclusion from the data in Fig. 4. This means that the CO_2 pulses must lead to the decomposition of surface species that can evolve additional CO_2, which will be discussed in the following.

More information on the consumption and formation of the different CO_2 isotopomers can be obtained from inspecting the accumulation of these species during $C^{18}O_2$ pulsing. The consumption of $C^{18}O_2$ molecules, which was calculated from the difference between incoming $C^{18}O_2$ pulses (brown dotted line in Fig. S14a and e) and the detected $C^{18}O_2$ signals (Fig. 6a, S14a) and which is indicated by the bright green line in Fig. 6b, increased rapidly in the beginning. Subsequently, the increase slowed down soon, reflecting the rapidly increasing $C^{18}O_2$ pulse size in Fig. 6a. The continuous increase of the integrated intensity of the $C^{18}O_2$ pulses differs distinctly from the rapid saturation of the CO_2 pulses observed during $C^{16}O_2$ pulsing (Fig. 4a).

$C^{16}O_2$ formation (dark green dotted line in Fig. 6b) also starts at the very beginning of the sequence. In this initial phase, $C^{16}O_2$ formation corresponds quantitatively to $C^{18}O_2$ consumption. Hence, within the precision of the experiment all $C^{18}O_2$ consumed is released as $C^{16}O_2$, reflecting complete exchange of the oxygen in CO_2 in this phase. Subsequently, the increase of the $C^{16}O_2$ signal bends off, i.e., an increasing amount of the ^{18}O in $C^{18}O_2$ is not exchanged against ^{16}O. For longer times, after about 400 pulses, the contribution of $C^{16}O_2$ becomes rather small and the $C^{16}O_2$ formation approaches a limiting value, indicating that complete oxygen exchange becomes smaller and smaller and finally negligible. Here it is important to note that in these experiments we cannot discriminate between exchange with surface atoms of the catalyst support and O-exchange with adsorbed species that are present on the surface, such as surface carbonates. Considering, however, that according to the TPD experiment there are considerable amounts of ad-species on the surface that can decompose to CO_2 such as surface carbonates (Fig. 3), and the high stability of the Al_2O_3 support, we strongly favor the latter explanation. For simplicity, unless specified explicitly, we will refer to these species as 'exchangeable O atoms'. Finally, the formation of the mixed isotopomer $C^{16}O^{18}O$ (dark blue dotted line in Fig. 6b) is negligible at the beginning, but then increases steadily and increasingly dominates the observed CO_2 formation. It is the dominant contribution after about 300 pulses.

The trends observed during $C^{18}O_2$ pulsing can simply be explained by an exchange mechanism, assuming that O-exchange with the catalyst surface/adspecies can occur repeatedly. While initially there are only ^{16}O or ^{16}O containing adsorbed species in / on the surface, exchange with ^{18}O during $C^{18}O_2$ pulsing will result in an increasing content of ^{18}O isotopes. Accordingly, at the beginning of the pulse sequence, repeated reactive interaction of $C^{18}O_2$ with the catalyst surface should result in the formation of $C^{16}O_2$ only, since the probability of exchanging with an ^{18}O atom on/in the surface is negligible. With increasing ^{18}O content, the probability of exchanging with an ^{18}O atom increases, and accordingly also the chances for $C^{18}O^{16}O$ formation. In the same way, only less pronounced, also the formation of $C^{18}O_2$ will occur. For a random distribution of the ^{18}O atoms in the surface, repeated O-exchange for each CO_2 molecule in the catalyst bed and a relative ^{18}O content of x in the exchangeable surface oxygen species we would expect a product distribution of x^2 $C^{18}O_2$, $(2x\text{-}2x^2)$ $C^{18}O^{16}O$ and $(1\text{-}x)^2$ $C^{16}O_2$ (see Fig. S15). This means that the measured $C^{18}O_2$ pulses i) consist (mainly) of CO_2 species that have exchanged ^{18}O with the catalyst surface, and that ii) this fraction increases considerably with increasing ^{18}O content in the exchangeable O-atoms, while initially this content is negligible. Correspondingly, the relative amount of $C^{18}O^{16}O$ and $C^{16}O_2$ should decrease with time and be negligible close to complete exchange. At the end of the experiment illustrated in Fig. 6 the relative ^{16}O content of the exchangeable oxygen should be somewhere between $x = 0.75$ and $x = 1.0$, where the content of $C^{16}O_2$ is rather small and the content of $C^{18}O_2$ is higher than that of the mixed isotopomer $C^{18}O^{16}O$.

The excess of CO_2 molecules can be quantified by comparing the accumulated consumption (calculation see above) and formation of the different CO_2 isotopomers. The relative amount of excess CO_2 formation during CO_2 pulsing is obtained from the data in Fig. 6c, where we plotted the number of $C^{18}O_2$ molecules entering the catalyst bed (purple) and the number of CO_2 molecules detected after passing through the catalyst bed (olive). The latter data are obtained by integration of the number of the different isotopomers detected in the effluent pulses as indicated in Fig. S14e. The data indicate that during most of the pulse sequence approx. 1.15–1.3 CO_2 molecules are released for each incoming CO_2 molecule, which is indicated by the blue dotted line in Fig. 6c.

Furthermore, the data can also provide a reasonable explanation for why it was not possible to detect the O_{act} formation from the consumption of CO_2 during CO_2 pulsing (Fig. 4). First of all, the deposition of O_{act} per pulse is only small and distributed over many pulses, and second it is even overcompensated by the formation of CO_2 by decomposition of adsorbed species such as surface carbonates. This latter process can be rationalized when considering that during the preceding reduction of the catalyst by CO pulsing surface carbonates were formed as well (see Fig. 2), until reaching a dynamic equilibrium state. The same is possible also for CO_2 pulsing. If the steady-state concentration of surface carbonates resulting from CO pulsing at 190 °C is higher than the

steady-state concentration obtained during CO_2 pulsing, sending CO_2 pulses on a sample that had before been exposed to CO pulses will lead to a decay of the amount of surface carbonates and thus to additional CO_2 formation, as observed experimentally. This is supported also by the fact that the total number of excess CO_2 molecules detected in Fig. 6c (3.3×10^{20} molecules g_{cat}^{-1}) is in the same order of magnitude as the numbers derived for carbonate formation during CO pulsing (2.4×10^{20} molecules g_{cat}^{-1}) and from the TPD measurement after CO pulsing (2.1×10^{20} molecules g_{cat}^{-1}). Of course, this also means that the formation of excess CO_2 during CO_2 pulsing is of transient nature and will decay with decreasing amount of surface carbonates on the catalyst. The fact that in the later stages of the experiment in Fig. 6 the CO_2 excess becomes rather small, as indicated by the similar slope of the lines in Fig. 6c, indicates that this limit was almost reached in the present experiment.

In total, these data clearly indicate that the amount of released CO_2 will differ from that in the incoming CO_2 pulses due to two simultaneously occurring processes, O_{act} deposition (consumption of CO_2) and surface carbonate decomposition (release of CO_2). Both effects are most pronounced in the initial phase of CO pulsing, while later, when approaching steady state conditions, CO_2 consumption and formation should be of similar magnitude. This is illustrated also by the turquoise dotted line in Fig. 6b, which indicates the sum of $C^{18}O^{16}O$ and $C^{18}O_2$ formation. It clearly deviates most from $C^{18}O_2$ consumption in the early stages of the pulse sequence.

These results can be compared with data reported by Guerrero-Ruiz et al., who found that exposing a reduced Ru/Al_2O_3 catalyst to $C^{18}O_2$ or a mixture of $C^{18}O_2$ and $^{16}O_2$ results in isotope mixing in CO_2, where all three isotopomers are observed, while there is no isotope mixing for O_2 [63]. The authors explained this by the formation of surface carbonate species, which facilitate oxygen exchange with CO_2. Since in this case all three isotopomers were observed, while over SiO_2 only $^{18}O_2$ and $C^{18}O^{16}O$ were observed. They furthermore suggested that different carbonate species are formed on these two oxides, a polydentate species on Al_2O_3 and a bidentate species. In the presence of Ru nanoparticles, over a 0.64 wt% Ru/Al_2O_3 catalyst, exposure to a mixture of $C^{18}O_2$ and $^{16}O_2$ caused oxygen exchange also in O_2, which may be due to a combination of O_2 stimulated decomposition of surface carbonates and carbonate formation from $C^{18}O_2$. While these experiments were performed at significantly higher temperature (450 °C), the trends are nevertheless comparable with our findings, indicating that exchange is rather efficient and that kinetic limitations are small, at least at the higher temperature.

The carbonate pathway proposed for oxygen exchange differs from a proposal by Yan et al. [64]. They observed the formation of $C^{18}O$ and $H_2^{18}O$ when flowing a $H_2/C^{18}O_2$ mixture over a pre-reduced 1 wt% Ru/Al_2O_3 catalyst, in addition to CH_4, CO, and H_2O. Based on density functional theory (DFT) calculations they proposed that the oxygen exchange proceeds via the formation of Ru-^{18}O-Al-bonds at the interface of Ru nanoparticle and support during the dissociative adsorption of CO_2. This would not be consistent, however, with our TAP observation of an excess of CO_2 formation during CO_2 pulsing, which leads us to favor the carbonate pathway as dominant pathway for the oxygen exchange between CO_2 and the Ru/Al_2O_3 catalyst.

Using isotope marked $C^{18}O_2$ we could demonstrate in this section that the interaction between CO_2 and the reduced Ru/Al_2O_3 catalyst leads to a reversible exchange of active oxygen between catalyst surface and CO_2. Most likely, the proposed oxygen deposition / removal proceeds either via the exchange of O_{act} between CO_2 and surface carbonate species, or, alternatively, by the formation and (CO_2 induced) decomposition of carbonates. Quantitative evaluation of the consumption and release of the different CO_2 isotopomers confirmed that CO_2 pulsing on confirms the above conclusion. The trends can be explained by an increasing conversion of the initial $C^{16}O_3$ carbonate species into $C^{16}O_x^{18}O_3$ and finally into $C^{18}O_3$ type species, in addition to increasing carbonate decomposition.

4. Discussion

The data presented in the preceding sections, mainly TAP reactor multi-pulse and TAP-TPD experiments investigating the interaction of CO_2 with a $Ru/\gamma\text{-}Al_2O_3$ catalyst, led to the following conclusions on the deposition of active oxygen (O_{act}) upon interaction of the catalyst with these gases and on the reaction between CO_2 and adsorbed species such as surface carbonates. For comparison, we also include measurements on O_{act} deposition from O_2 pulses:

- Multi-pulse TAP reactor measurements indicate that the interaction of CO_2 with a pre-reduced $Ru/\gamma\text{-}Al_2O_3$ catalyst leads to the re-oxidation of the catalyst, forming catalytically active oxygen (O_{act}) species. These are different from the inert oxygen species in the $\gamma\text{-}Al_2O_3$ support, as they can be removed again by CO pulses. This closely resembles the O_{act} deposition behavior during O_2 pulsing, at least on a qualitative basis.
- Based on the O_2 consumption during O_2 pulses, exposure to O_2 pulses can fully oxidize the Ru nanoparticles in a very efficient way under present reaction conditions, up to RuO_2. Subsequent reduction by CO pulses is equally efficient, also with complete conversion of the pulses in the initial phase. On the other hand, the O_{act} deposition from CO_2 is significantly slower than from O_2 pulses and could not be detected by direct evaluation, from the difference between incoming and effluent pulses, but only by CO pulse titration of the deposited O_{act}. In contrast, the difference in the total amount of O_{act} deposited is less drastic (about 58% of that obtained during O_2 pulsing after 540 pulses).
- In the presence of CO, the deposition of active oxygen from CO_2 is even less efficient, presumably due to the competing removal of O_{act} by CO. In the presence of H_2, in contrast, deposition of O_{act} is higher again, even higher than for CO_2 alone, most likely due to the formation of highly reactive H_2O via the RWGS reaction.
- Comparing the amount of CO consumption and CO_2 formation upon exposure of the pre-oxidized $Ru/\gamma\text{-}Al_2O_3$ catalyst to CO pulses shows a significant deficit in CO_2 product molecules. This is attributed to the formation of surface carbonate species. Since earlier FTIR studies had shown that surface carbonate species are adsorbed on the Al_2O_3 support [65] these observations indicate that CO_2 molecules formed from CO pulsed and O_{act} react with oxygen on the support either at the interface between Ru nanoparticles and support, or after spill-over of adsorbed CO_2 to the support, or after or desorption / re-adsorption of CO_2.
- On the other hand, exposing the pre-reduced catalyst (pre-reduction by CO pulses) to CO_2 pulses, we find a net excess of CO_2 formation, in addition to slow O_{act} build-up. We explain the excess of CO_2 by a CO_2-induced decomposition of surface carbonates that had been formed during the preceding reduction by CO pulses. On the other hand, two FTIR spectroscopy studies reported that the interaction of CO_2 with a Ru/Al_2O_3 catalyst that was reduced in H_2 rather than in CO and thus has a low amount of surface carbonates leads to the formation of surface carbonates [65,66]. The apparent controversy can be resolved when assuming that the dominant effect of the interaction of CO_2 with the catalyst surface depends on the amount of surface carbonate species present on the catalyst surface. While for surfaces with a low amount of pre-existing surface carbonates interaction with CO_2 leads to carbonate formation, the opposite (carbonate decomposition) is true for high amounts of pre-existing surface carbonates under present reaction conditions. This continues until steady state conditions are reached during CO_2 exposure.

  This idea is consistent also with our observation that interaction of CO with a O150 pre-oxidized Ru/Al_2O_3 catalyst, which has a relatively low content of surface carbonates, leads to surface carbonate formation, by reaction of the resulting CO_2 with the catalyst surface.
- The conclusion of surface carbonate formation upon interaction of the Ru/Al_2O_3 catalyst with CO or CO_2 pulses is supported by the

results of TPD experiments and XPS measurements. TPD spectra show a pronounced formation of CO_2 in the temperature range of 190–450 °C, with two distinct desorption maxima at 276 °C and 407 °C. These point to the existence of two slightly different states. XPS measurements are consistent with the presence of significant amounts of surface carbonates after CO pulsing

- This idea of a reversible surface carbonate formation / decomposition upon interaction with CO_2 is further supported by results of isotope labelling experiments, which showed that CO_2 efficiently exchanges oxygen with the catalyst surface, leading to the formation of $C^{16}O_2$ and $C^{18}O^{16}O$ upon $C^{18}O_2$ pulsing. Since oxygen in Al_2O_3 is considered as inert, we attribute this to oxygen exchange with surface carbonate species that had been formed during the preceding reduction of the initially oxidized catalyst by CO pulsing. Most simply, oxygen exchange with surface carbonates can proceed via continuous CO_2-induced decomposition and formation of surface carbonates. Also these experiments show a net excess of CO_2 formation. The relative intensities of the three isotopomers $C^{16}O_2$, $C^{18}O^{16}O$ and $C^{18}O_2$ and their variation with time fit to a model assuming random distribution of the different oxygen isotopes ^{16}O and ^{18}O on the surface during the pulse sequence, and repeated interaction and oxygen exchange between CO_2 and surface carbonate while the gas pulse passes through the catalyst bed.
- The observation of methane formation in mixed CO_2/H_2 pulses indicates that despite the existing pressure gap compared to realistic reaction conditions, the present findings are relevant also for the reaction behavior under realistic flow-reaction conditions.

Finally, more generally these findings are highly relevant for catalytic reactions on supported Ru catalysts involving the reduction of CO_2 such as the CO_2 methanation reaction or the RWGS reaction. Both play an important role for the efficient production of value-added feedstocks from CO_2 aiming to close the carbon cycle in the area of energy production and use.

5. Conclusion

Aiming at a detailed understanding of catalytic reactions involving CO_2, e.g., CO_2 methanation or the RWGS reaction, we have investigated the interaction of CO_2 and gas mixtures of CO_2 and a reducing gas, either CO or H_2, with a $Ru/\gamma\text{-}Al_2O_3$ catalyst by TAP reactor experiments. Multi-pulse experiments demonstrated that CO_2 can deposit active oxygen (O_{act}) on the catalyst, more specifically, on the Ru nanoparticle surface. The addition of CO reduced the efficiency of O_{act} deposition by CO_2, due to a competing O_{act} removal by reaction with CO. On the other hand, it was significantly increased in the presence of H_2, to a level comparable to that for O_{act} deposition upon O_2 pulsing. We explained this behavior by the formation of highly active water species via the RWGS reaction. Finally, combined results of TAP multi-pulse experiments using isotope marked $C^{18}O_2$, TAP-TPD and XPS measurements showed the build-up of a carbonate ad-layer on the catalyst surface during CO or CO_2 pulsing, which can be decomposed upon exposure to O_2 or CO_2 pulses.

In total, these quantitative TAP reactor results revealed that the interaction of Ru, more specifically of a Ru/Al_2O_3 catalyst, with CO_2 is highly complex and affects both the oxidation state of Ru as well as the amount of adsorbed surface carbonates and related species under reaction conditions.

Authors contributions

All authors contributed to the writing and have given approval to the final version of the manuscript.

Declaration of Competing Interest

The authors declare that they have no known competing financial interests or personal relationships that could have appeared to influence the work reported in this paper.

Data availability

Data will be made available on request.

Acknowledgements

We gratefully acknowledge Dr. Joachim Bansmann (Institute of Surface Chemistry and Catalysis, Ulm University) for XPS measurements.

Appendix A. Supporting information

Supplementary data associated with this article can be found in the online version at doi:10.1016/j.apcatb.2023.122817.

References

[1] G.A. Mills, F.W. Steffgen, Catalytic methanation, Catal. Rev. 8 (1974) 159–210, https://doi.org/10.1080/01614947408071860.
[2] P.J. Lunde, F.L. Kester, Carbon dioxide methanation on a ruthenium catalyst, Ind. Eng. Chem. Process Des. Dev. 13 (1974) 27–33, https://doi.org/10.1021/i260049a005.
[3] F. Solymosi, A. Erdöhelyi, M. Kocsis, Methanation of CO_2 on supported ru catalysts, J. Chem. Soc., Faraday Trans. 1: Phys. Chem. Condens. Phases 77 (1981) 1003–1012, https://doi.org/10.1039/F19817701003.
[4] V. Ponec, Carbon monoxide and carbon dioxide hydrogenation, in: G. Ertl, H. Knözinger, J. Weitkamp (Eds.), Handbook of Heterogeneous Catalysis, Wiley VCH, 1997, pp. 1876–1893.
[5] W. Wang, S. Wang, X. Ma, J. Gong, Recent advances in catalytic hydrogenation of carbon dioxide, Chem. Soc. Rev. 40 (2011) 3703–3727, https://doi.org/10.1039/c1cs15008a.
[6] J. Ashok, S. Pati, P. Hongmanorom, Z. Tianxi, C. Junmei, S. Kawi, A review of recent catalyst advances in CO_2 methanation processes, Catal. Today 356 (2020) 471–489, https://doi.org/10.1016/j.cattod.2020.07.023.
[7] C.H. Tan, S. Nomanbhay, A.H. Shamsuddin, Y.K. Park, H. Hernández-Cocoletzi, P. L. Show, Current developments in catalytic methanation of carbon dioxide - a review, Front. Energy Res. 9 (2022) 1–7, https://doi.org/10.3389/fenrg.2021.795423.
[8] T. Schaaf, J. Grünig, M.R. Schuster, T. Rothenfluh, A. Orth, Methanation of CO_2 - storage of renewable energy in a gas distribution system, Energy Sustain. Soc. 4 (2014) 1–14, https://doi.org/10.1186/s13705-014-0029-1.
[9] A. Rehmat, S.S. Randhava, Selective methanation of carbon monoxide, Ind. Eng. Chem. Prod. Res. Dev. 9 (1970) 512–515, https://doi.org/10.1021/i360036a009.
[10] S. Eckle, H.G. Anfang, R.J. Behm, What drives the selectivity for CO methanation in the methanation of CO_2-rich reformate gases on supported Ru catalysts? Appl. Catal. A Gen. 391 (2011) 325–333, https://doi.org/10.1016/j.apcata.2010.07.025.
[11] S. Tada, R. Kikuchi, Mechanistic study and catalyst development for selective carbon monoxide methanation, Catal. Sci. Technol. 5 (2015) 3061–3070, https://doi.org/10.1039/c5cy00150a.
[12] M.A. Vannice, The Catalytic Synthesis of Hydrocarbons from H_2/CO Mixtures over the Group VIII metals - I. The Specific Activities and Product Distributions of Supported Metals, J. Catal. 50 (1977) 228–236, https://doi.org/10.1016/0021-9517(77)90031-8.
[13] V. Ponec, Some aspects of the mechanism of methanation and Fischer-Tropsch synthesis, Catal. Rev. Sci. Eng. 18 (1978) 151–171, https://doi.org/10.1080/03602457808067530.
[14] A.T. Bell, Catalytic synthesis of hydrocarbons over group VIII metals. a discussion of the reaction mechanism, Catal. Rev. Sci. Eng. 23 (1981) 203–232, https://doi.org/10.1080/03602458108068076.
[15] H. Schulz, Short history and present trends of Fischer-Tropsch synthesis, Appl. Catal. A Gen. 186 (1999) 3–12, https://doi.org/10.1016/S0926-860X(99)00160-X.
[16] M. Claeys, R. Cowan, H. Schulz, Temporal changes of Fischer-Tropsch activity and selectivity using ruthenium, Top. Catal. 26 (2003) 139–143, https://doi.org/10.1023/B:TOCA.0000012994.27890.4c.
[17] J.J.H.M. Font Freide, T.D. Gamlin, C. Graham, J.R. Hensman, B. Nay, C. Sharp, An adventure in catalysis: the story of the BP Fischer-Tropsch catalyst from laboratory to full-scale demonstration in Alaska, Top. Catal. 26 (2003) 3–12, https://doi.org/10.1023/B:TOCA.0000012982.48191.ab.
[18] R.W. Dorner, D.R. Hardy, F.W. Williams, H.D. Willauer, Heterogeneous catalytic CO_2 conversion to value-added hydrocarbons, Energy Environ. Sci. 3 (2010) 884–890, https://doi.org/10.1039/c001514h.
[19] A. Aitbekova, L. Wu, C.J. Wrasman, A. Boubnov, A.S. Hoffman, E.D. Goodman, S. R. Bare, M. Cargnello, Low-temperature restructuring of CeO_2-Supported Ru nanoparticles determines selectivity in CO_2 catalytic reduction, J. Am. Chem. Soc. 140 (2018) 13736–13745, https://doi.org/10.1021/jacs.8b07615.
[20] M. Zhu, Q. Ge, X. Zhu, Catalytic reduction of CO_2 to CO via Reverse Water Gas Shift Reaction: Recent advances in the design of active and selective supported metal

catalysts, Trans. Tianjin Univ. 26 (2020) 172–187, https://doi.org/10.1007/s12209-020-00246-8.
[21] R. Tang, Z. Zhu, C. Li, M. Xiao, Z. Wu, D. Zhang, C. Zhang, Y. Xiao, M. Chu, A. Genest, G. Rupprechter, L. Zhang, X. Zhang, L. He, Ru-catalyzed reverse water gas shift reaction with near-unity selectivity and superior stability, ACS Mater. Lett. 3 (2021) 1652–1659, https://doi.org/10.1021/acsmaterialslett.1c00523.
[22] M.R. Prairie, A. Renken, J.G. Highfield, K. Ravindranathan Thampi, M. Grätzel, A. Fourier transform, infrared spectroscopic study of CO_2 methanation on supported ruthenium, J. Catal. 129 (1991) 130–144, https://doi.org/10.1016/0021-9517(91)90017-X.
[23] K. Yaccato, R. Carhart, A. Hagemeyer, A. Lesik, P. Strasser, A.F. Volpe Jr., H. Turner, H. Weinberg, R.K. Grasselli, C. Brooks, Competitive CO and CO_2 methanation over supported noble metal catalysts in high throughput scanning mass spectrometer, Appl. Catal. A Gen. 296 (2005) 30–48, https://doi.org/10.1016/j.apcata.2005.07.052.
[24] S. Eckle, H.G. Anfang, R.J. Behm, Reaction intermediates and side products in the methanation of CO and CO_2 over supported Ru catalysts in H_2-rich reformate gases, J. Phys. Chem. C. 115 (2011) 1361–1367, https://doi.org/10.1021/jp108106t.
[25] H. Over, Ruthenium dioxide, a fascinating material for atomic scale surface chemistry, Appl. Phys. A Mater. Sci. Process 75 (2002) 37–44, https://doi.org/10.1007/s003390101053.
[26] H. Over, A.P. Seitsonen, Oxidation of metal surfaces, Science 297 (2002) 2003–2005, https://doi.org/10.1126/science.1077063.
[27] R.R. Ford, Carbon monoxide adsorption on the transition metals, Adv. Catal. 21 (1970) 51–150, https://doi.org/10.1016/S0360-0564(08)60564-7.
[28] E. Zağli, J.L. Falconer, Carbon dioxide adsorption and methanation on ruthenium, J. Catal. 69 (1981) 1–8, https://doi.org/10.1016/0021-9517(81)90122-6.
[29] F. Solymosi, The bonding, structure and reactions of CO_2 adsorbed on clean and promoted metal surfaces, J. Molec. Catal. 65 (1991) 337–358, https://doi.org/10.1016/0304-5102(91)85070-I.
[30] M. Pachecka, J.M. Sturm, C.J. Lee, F. Bijkerk, Adsorption and dissociation of CO_2 on Ru(0001), J. Phys. Chem. C. 121 (2017) 6729–6735, https://doi.org/10.1021/acs.jpcc.7b00021.
[31] H.Y.T. Chen, S. Tosoni, G. Pacchioni, Adsorption of ruthenium atoms and clusters on anatase TiO_2 and tetragonal ZrO_2(101) surfaces: a comparative DFT study, J. Phys. Chem. C. 119 (2015) 10856–10868, https://doi.org/10.1021/jp510468f.
[32] S. Chen, A.M. Abdel-Mageed, M. Li, S. Cisneros, J. Bansmann, J. Rabeah, A. Brückner, A. Groß, R.J. Behm, Electronic metal-support interactions and their promotional effect on CO_2 methanation on Ru/ZrO_2 catalysts, J. Catal. 400 (2021) 407–420, https://doi.org/10.1016/j.jcat.2021.06.028.
[33] Y. Li, Y. Zhang, K. Qian, W. Huang, Metal-support interactions in metal/oxide catalysts and oxide-metal interactions in oxide/metal inverse catalysts, ACS Catal. 12 (2022) 1268–1287, https://doi.org/10.1021/acscatal.1c04854.
[34] S. Chen, A.M. Abdel-Mageed, C. Gauckler, S.E. Olesen, I. Chorkendorff, R.J. Behm, Selective CO methanation on isostructural Ru nanocatalysts: the role of support effects, J. Catal. 373 (2019) 103–115, https://doi.org/10.1016/j.jcat.2019.03.015.
[35] F. Wang, C. Li, X. Zhang, M. Wei, D.G. Evans, X. Duan, Catalytic behavior of supported Ru nanoparticles on the {100}, {110}, and {111} facet of CeO_2, J. Catal. 329 (2015) 177–186, https://doi.org/10.1016/j.jcat.2015.05.014.
[36] A.M. Abdel-Mageed, K. Wiese, A. Hauble, J. Bansmann, J. Rabeah, M. Parlinska-Wojtan, A. Brückner, R.J. Behm, Steering the selectivity in CO_2 reduction on highly active Ru/TiO_2 catalysts: Support particle size effects, J. Catal. 401 (2021) 160–173, https://doi.org/10.1016/j.jcat.2021.07.020.
[37] S. Chen, A.M. Abdel-Mageed, M. Dyballa, M. Parlinska-Wojtan, J. Bansmann, S. Pollastri, L. Olivi, G. Aquilanti, R.J. Behm, Raising the CO_x methanation activity of a Ru/γ-Al_2O_3 catalyst by activated modification of metal–support interactions, Angew. Chem. Int. Ed. 59 (2020) 22763–22770, https://doi.org/10.1002/anie.202007228.
[38] S. Eckle, Y. Denkwitz, R.J. Behm, Activity, selectivity, and adsorbed reaction intermediates/reaction side products in the selective methanation of CO in reformate gases on supported Ru catalysts, J. Catal. 269 (2010) 255–268, https://doi.org/10.1016/j.jcat.2009.10.025.
[39] A.M. Abdel-Mageed, D. Widmann, S. Eckle, R.J. Behm, Improved performance of Ru/γ-Al_2O_3 catalysts in the selective methanation of CO in CO_2-rich reformate gases upon transient exposure to water-containing reaction gas, ChemSusChem 8 (2015) 3869–3881, https://doi.org/10.1002/cssc.201500883.
[40] A.M. Abdel-Mageed, S. Eckle, D. Widmann, R.J. Behm, Water assisted dispersion of ru nanoparticles: the impact of water on the activity and selectivity of supported Ru catalysts during the selective methanation of CO in CO_2-rich reformate, J. Catal. 335 (2016) 79–94, https://doi.org/10.1016/j.jcat.2015.12.013.
[41] A.M. Abdel-Mageed, D. Widmann, S.E. Olesen, I. Chorkendorff, J. Biskupek, R. J. Behm, Selective CO methanation on Ru/TiO_2 catalysts: role and influence of metal-support interactions, ACS Catal. 5 (2015) 6753–6763, https://doi.org/10.1021/acscatal.5b01520.
[42] A.M. Abdel-Mageed, K. Wiese, M. Parlinska-Wojtan, J. Rabeah, A. Brückner, R. J. Behm, Encapsulation of Ru nanoparticles: Modifying the reactivity toward CO and CO_2 methanation on highly active Ru/TiO_2 catalysts, Appl. Catal. B Environ. 270 (2020), 118846, https://doi.org/10.1016/j.apcatb.2020.118846.
[43] R. Leppelt, D. Hansgen, D. Widmann, T. Häring, G. Bräth, R.J. Behm, Design and characterization of a temporal analysis of products reactor, Rev. Sci. Instrum. 78 (2007), 104103, https://doi.org/10.1063/1.2791948.
[44] J.T. Gleaves, G.S. Yablonskii, P. Phanawadee, Y. Schuurman, TAP-2: an interrogative kinetics approach, 1997. doi: Appl. Catal. A Gen. 160 (1997) 55–88, https://doi.org/10.1016/S0926-860X(97)00124-5.
[45] J.F. Moulder, W.F. Stickle, P.E. Sobol, K.D. Bomben, Handbook of X-ray photoelectron spectroscopy, 2nd ed., Perkin-Elmer Corporation, Eden Prairie, Minn. (1992), https://doi.org/10.1002/0470014229.ch22.
[46] D.J. Morgan, Resolving ruthenium: XPS studies of common ruthenium materials, Surf. Interf. Anal. 47 (2015) 1072–1079, https://doi.org/10.1002/sia.5852.
[47] J. Wang, C.Y. Fan, K. Jacobi, G. Ertl, Adsorption and reaction of CO on RuO_2(110) surfaces, Surf. Sci. 481 (2001) 113–118, https://doi.org/10.1016/S0039-6028(01)01017-2.
[48] J. Aßmann, V. Narkhede, N.A. Breuer, M. Muhler, A.P. Seitsonen, M. Knapp, D. Crihan, A. Farkas, G. Mellau, H. Over, Heterogeneous oxidation catalysis on ruthenium: bridging the pressure and materials gaps and beyond, J. Phys. Condens. Matter 20 (2008), 184017, https://doi.org/10.1088/0953-8984/20/18/184017.
[49] L.C. Wang, M. Tahvildar Khazaneh, D. Widmann, R.J. Behm, TAP reactor studies of the oxidizing capability of CO_2 on a Au/CeO_2 Catalyst – a first step toward identifying a redox mechanism in the reverse water–gas shift reaction, J. Catal. 302 (2013) 20–30, https://doi.org/10.1016/j.jcat.2013.02.021.
[50] L.C. Wang, D. Widmann, R.J. Behm, Reactive removal of surface oxygen by H_2, CO and CO/H_2 on a Au/CeO_2 catalyst and its relevance to the preferential CO oxidation (PROX) and reverse water gas shift (RWGS) reaction, Catal. Sci. Technol. 5 (2015) 925–941, https://doi.org/10.1039/c4cy01030b.
[51] D. Widmann, R.J. Behm, Active oxygen on a Au/TiO_2 catalyst: formation, stability, and CO oxidation activity, Angew. Chem. Int. Ed. 50 (2011) 10241–10245, https://doi.org/10.1002/anie.201102062.
[52] L.C. Wang, Y. Zhong, D. Widmann, J. Weissmüller, R.J. Behm, On the role of residual ag in nanoporous Au catalysts for CO oxidation: a combined microreactor and TAP reactor study, ChemCatChem 4 (2012) 251–259, https://doi.org/10.1002/cctc.201100297.
[53] K. Wiese, A.M. Abdel-Mageed, A. Klyushin, R.J. Behm, Dynamic Changes of Au/ZnO Catalysts during Methanol Synthesis: A model study by temporal analysis of products (TAP) and Zn LIII near edge X-ray absorption spectroscopy, Catal. Today 336 (2019) 193–202, https://doi.org/10.1016/j.cattod.2018.11.074.
[54] A.M. Abdel-Mageed, M. Büsselmann, K. Wiese, C. Fauth, R.J. Behm, Influence of water vapor on the performance of Au/ZnO catalysts in methanol synthesis from CO_2 and H_2: a high-pressure kinetic and TAP reactor study, Appl. Catal. B: Environ. 297 (2021), 120416, https://doi.org/10.1016/j.apcatb.2021.120416.
[55] G. Busca, V. Lorenzelli, Infrared spectroscopic identification of species arising from reactive adsorption of carbon oxides on metal oxide surfaces, Mater. Chem. 7 (1982) 89–126, https://doi.org/10.1016/0390-6035(82)90059-1.
[56] Y. Pan, C. Liu, Q. Ge, Adsorption and protonation of CO_2 on partially hydroxylated γ-Al_2O_3 surfaces: a density functional theory study, Langmuir 24 (2008) 12410–12419, https://doi.org/10.1021/la802295x.
[57] K. Föttinger, R. Schlögl, G. Rupprechter, The mechanism of carbonate formation on Pd-Al_2O_3 catalysts, Chem. Comm. 3 (2008) 320–322, https://doi.org/10.1039/b713161e.
[58] C. Weilach, C. Spiel, K. Föttinger, G. Rupprechter, Carbonate formation on Al_2O_3 thin film model catalyst supports, Surf. Sci. 605 (2011) 1503–1509, https://doi.org/10.1016/j.susc.2011.05.025.
[59] X. Wang, Y. Hong, H. Shi, J. Szanyi, Kinetic modeling and transient DRIFTS–MS studies of CO_2 methanation over Ru/Al_2O_3 catalysts, J. Catal. 343 (2016) 185–195, https://doi.org/10.1016/j.jcat.2016.02.001.
[60] P. Dongapure, S. Bagchi, S. Mayadevi, R.N. Devi, Variations in activity of Ru/TiO_2 and Ru/Al_2O_3 catalysts for CO_2 hydrogenation: An investigation by in-situ infrared spectroscopy studies, Molec. Catal. 482 (2020) 1–6, https://doi.org/10.1016/j.mcat.2019.110700.
[61] J. Szanyi, J.H. Kwak, Dissecting the Steps of CO_2 Reduction: 1. The interaction of CO and CO_2 with γ-Al_2O_3: An in-situ FTIR study, Phys. Chem. Chem. Phys. 16 (2014) 15117–15125, https://doi.org/10.1039/c4cp00616j.
[62] G. Garbarino, D. Bellotti, E. Finocchio, L. Magistri, G. Busca, Methanation of carbon dioxide on Ru/Al_2O_3: catalytic activity and infrared study, Catal. Today 277 (2016) 21–28, https://doi.org/10.1016/j.cattod.2015.12.010.
[63] A. Guerrero-Ruiz, P. Ferreira-Aparicio, M.B. Bachiller-Baeza, I. Rodriguez-Ramos, Isotopic tracing experiments in syngas production from methane on Ru/Al_2O_3 and Ru/SiO_2, Catal. Today 46 (1998) 99–105, https://doi.org/10.1021/la970856q.
[64] Y. Yan, Q. Wang, C. Jiang, Y. Yao, D. Lu, J. Zheng, Y. Dai, H. Wang, Y. Yang, Ru/Al_2O_3 catalyzed CO_2 hydrogenation: oxygen-exchange on metal-support interfaces, J. Catal. 367 (2018) 194–205, https://doi.org/10.1016/j.jcat.2018.08.026.
[65] J. Zheng, C. Wang, W. Chu, Y. Zhou, K. Köhler, CO_2 methanation over supported Ru/Al_2O_3 catalysts: Mechanistic studies by *in situ* infrared spectroscopy, ChemistrySelect 1 (2016) 3197–3203, https://doi.org/10.1002/slct.201600651.
[66] P. Ferreira-Aparicio, C. Márquez-Alvarez, I. Rodríguez-Ramos, Y. Schuurman, A. Guerrero-Ruiz, C. Mirodatos, A transient kinetic study of the carbon dioxide reforming of methane over supported Ru catalysts, J. Catal. 184 (1999) 202–212, https://doi.org/10.1006/jcat.1999.2439.